LXX International conference "NUCLEUS – 2020. Nuclear physics and elementary particle physics. Nuclear physics technologies"

INVESTIGATION OF REACTION CROSS SECTIONS FOR BEAM OF ^{8}Li, ^{8}He ON ^{28}Si, ^{59}Co, ^{181}Ta TARGETS

Sobolev Yu.G., Stukalov S.S., Samarin V.V., Naumenko M.A., Penionzhkevich Yu.E.

FLEROV LABORATORY of NUCLEAR REACTIONS
Joint Institute for Nuclear Research, Dubna, Russia

Outline

- Motivation
- Experiment
- Fusion-evaporation calculations
- Data processing
- Theory:

  Structure of projectile nuclei ^{8}Li, ^{8}He

  Time-dependent Schrödinger equation approach
- Cross sections calculations:

  Neutron loss cross sections

  Total reaction cross sections

Total reaction cross sections for ^{11}Li + ^{28}Si compared with ^{9}Li + ^{28}Si

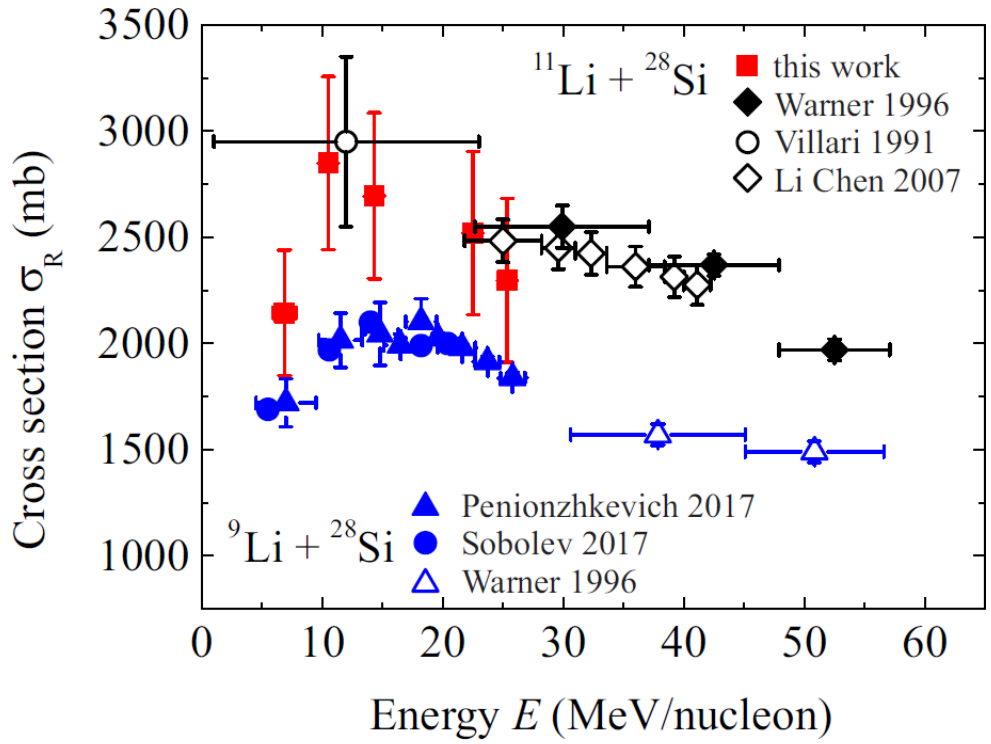

Yu. E. Penionzhkevich, Yu. G. Sobolev, V. V. Samarin, M. A. Naumenko, N. A. Lashmanov, V. A. Maslov, I. Sivá˘cek, and S. S. Stukalov. PHYSICAL REVIEW C 99, 014609 (2019)

Great enhancement is observed

R.E. Warner et al., Phys. Rev. C 54, 1700 (1996).

A.C.C. Villari et al., Phys. Lett. B 268, 345 (1991).

Li Chen et al., High Energy Phys. Nucl. Phys. 31, 1102 (2007).

Yu.G. Sobolev et al., Phys. Part. Nucl. 48, 922 (2017).

Yu.E. Penionzhkevich et al., Phys. Atom. Nucl. 80, 928 (2017).

Experimental charge radii [1], fm	
^{6}Li	2.589
^{7}Li	2.444
^{8}Li	2.339
^{9}Li	2.245
^{11}Li	2.482
^{4}He	1.6755
^{6}He	2.066
^{8}He	1.924

Motivation: what about ^{8}He, ^{8}Li?

[1] NRV web knowledge base on low-energy nuclear physics. URL: http://nrv.jinr.ru/

Experiment: a projectile nucleus beam

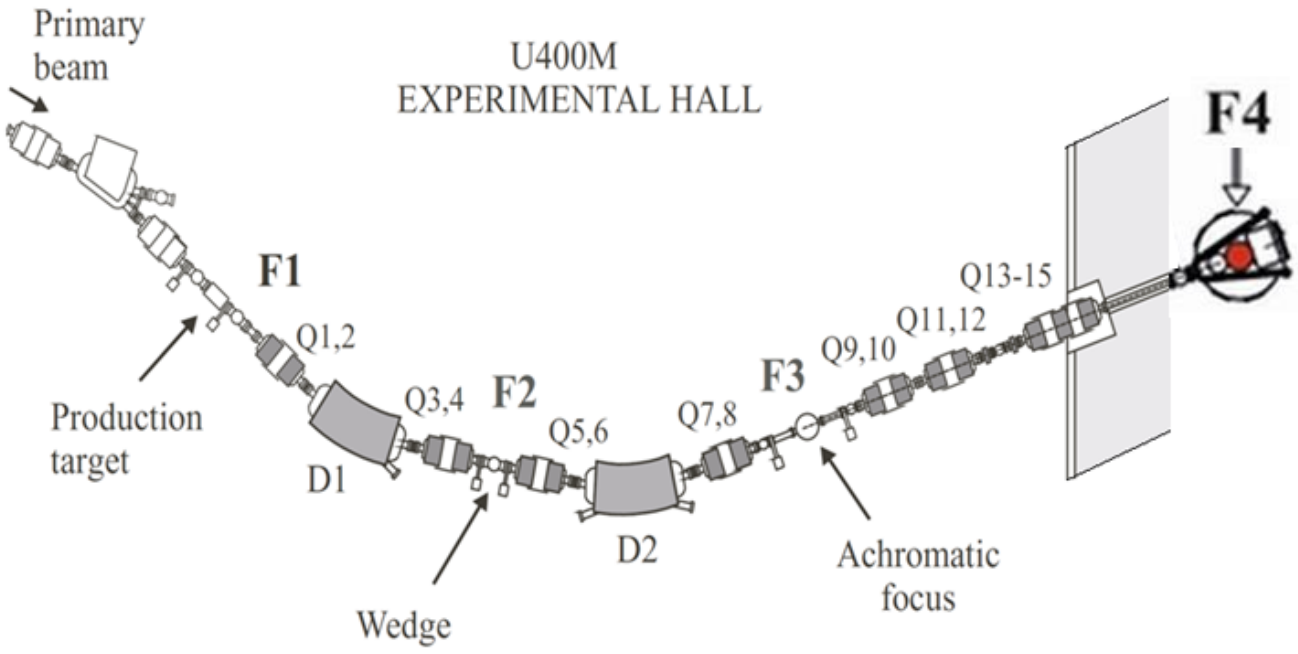

Parameter	Units	Value
Maximum magnetic rigidity	Tm	3.6
Solid angle	msr	0.9
Horizontal acceptance angle	mrad	20
Vertical acceptance angle	mrad	14
Momentum acceptance	%	4.2 - 8.4
Intermediate focal plane F2		
Horizontal magnification	-	0.5
Vertical magnification	-	2.0
Momentum dispersion	mm/%	4.0 - 18.0
Momentum resolution (FWHM) *)	-	$3x10^{-3}$
Achromatic focal plane F3		
Momentum dispersion	mm/%	-
Horizontal and vertical magnification	-	1.0
Horizontal RIB size (FWHM)	mm	8
Vertical RIB size (FWHM)	mm	10
Final focal plane F4		
Momentum dispersion	mm/%	-
Horizontal RIB size (FWHM)	mm	20
Vertical RIB size (FWHM)	mm	16
Horizontal acceptance	π×mm×mrad	60
Vertical acceptance	π×mm×mrad	43

Fig. 1. ACCULINNA Fragment Separator.
http://aculina.jinr.ru/a-1.html

F1 – object plane; F2 – intermediate dispersion plane; F3 – achromatic focal plane; F4 –second focal plane, D1 and D2 – magnets , Q1–Q15 – quadrupole lenses, Q9–Q15 – intermediate dispersive magnetic quadrupole lenses.

Experiment: target and multi-detector γ-spectrometer

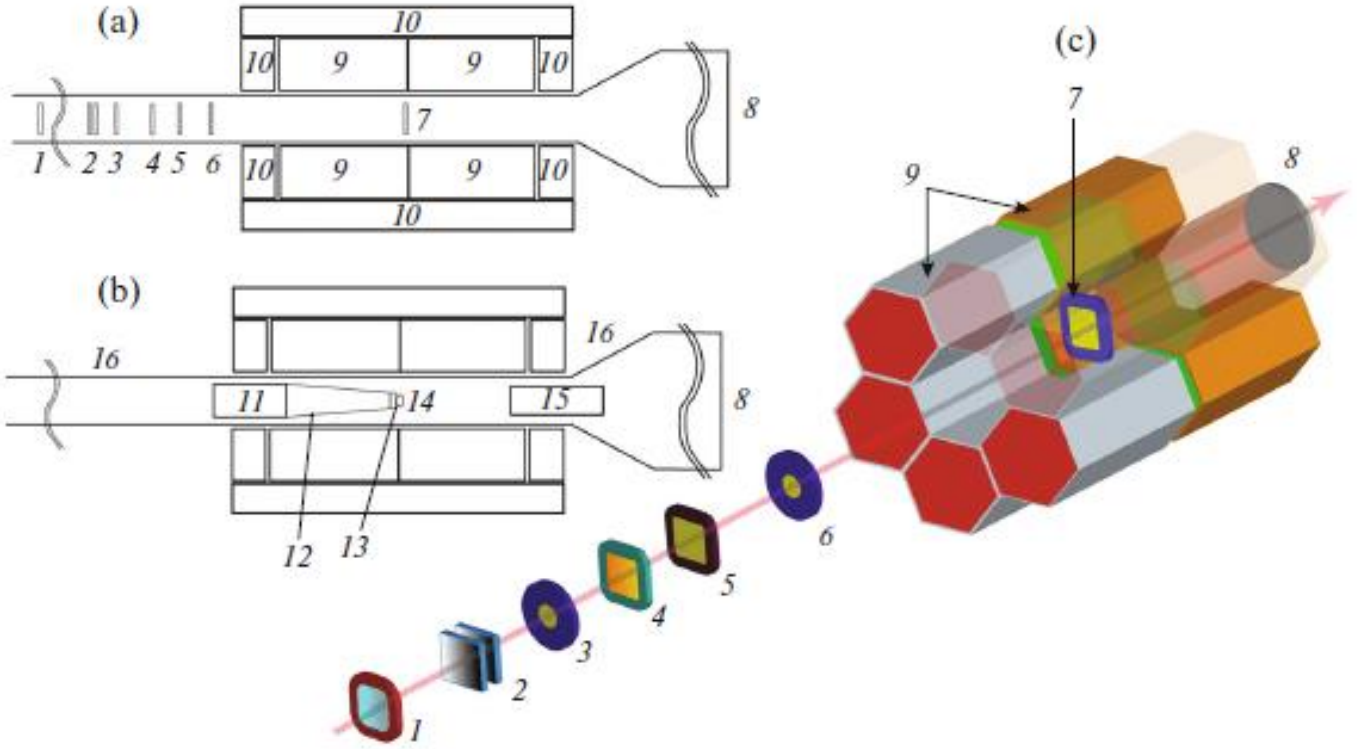

Fig. 2. Total reaction cross sections for interaction of ^{8}Li and ^{8}He secondary beam with ^{28}Si, ^{59}Co, ^{181}Ta target nuclei in the energy range 25–45 A MeV were measured. Modified transmission method based on registration of prompt *n*, γ radiation by a multi-detector γ-spectrometer [1, 2] was used. [1] *Yu.E. Penionzhkevich, Yu.G. Sobolev, V.V. Samarin, M.A. Naumenko, Phys. Rev. C. 2019. V.99. 014609.* [2] *Yu. G. Sobolev, Yu. E. Penionzhkevich, V. V. Samarin, M. A. Naumenko, S. S. Stukalov, I. Siváček, S. A. Krupko, A. Kugler, and J. Louko. Bulletin of the Russian Academy of Sciences: Physics, 2020, Vol. 84, No. 8, pp. 948–956.*

(c) Three-dimensional scheme of the experimental setup and its cross section during (a) measurements with a projectile nucleus beam and (b) calibration of the segmented spectrometer: (1) plastic scintillation detector; (2) polyethylene plates; (3) first active collimator; (4) ΔE strip Si-detector; (5) ΔE_0 start Si-detector; (6) second active collimator; (7) ^{28}Si, ^{59}Co, or ^{181}Ta target; (8) beam exit window; (9) scintillation CsI(Tl) detectors with PMTs; (10) Pb shielding; (11) PMT; (12) light reflector; (13) scintillator for detecting β-particles; (14) ^{60}Co source; (15) $CeBr_3$ detector; and (16) reaction chamber.

Calibration of the γ-spectrometer

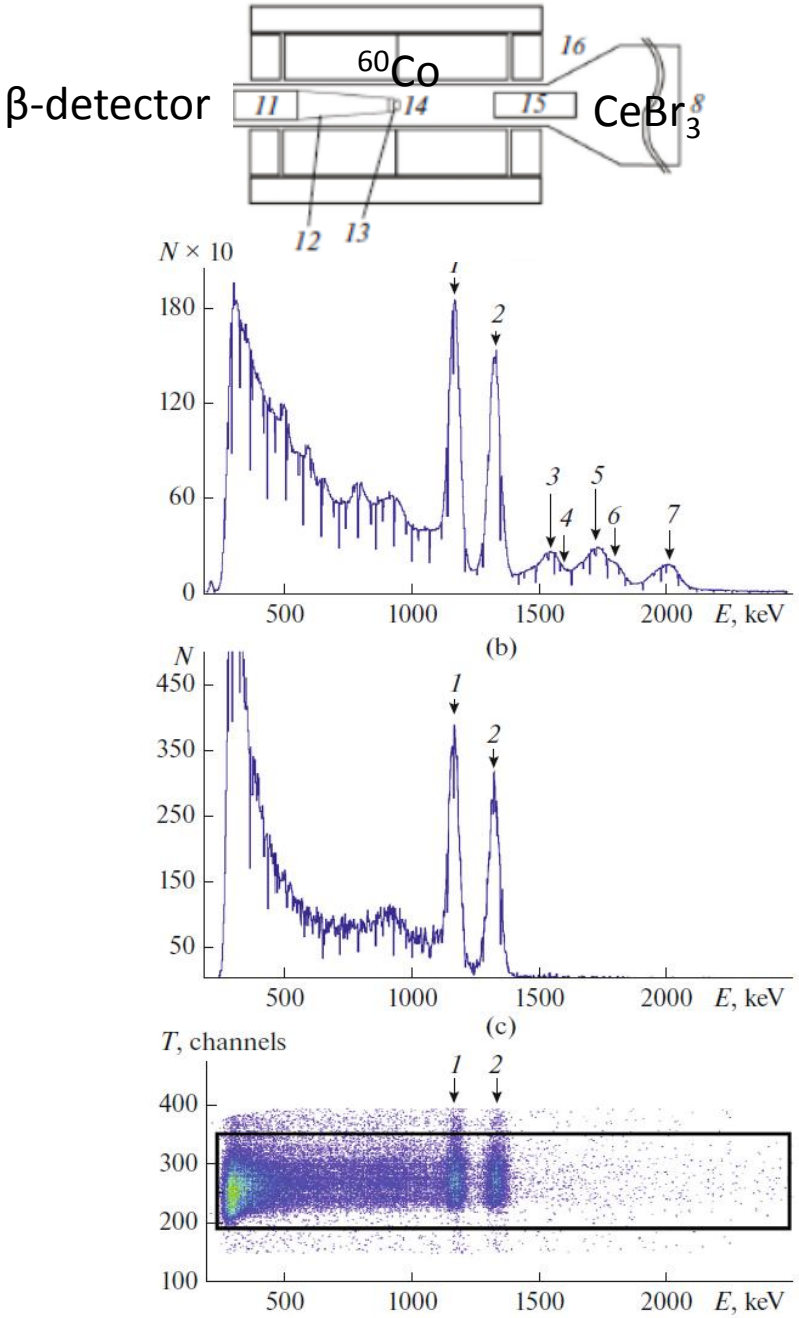

Fig. 3. (a) Inclusive energy spectrum of the $CeBr_3$ detector, obtained when calibrating the γ-spectrometer using a ^{60}Co source. (b) Energy spectrum of the $CeBr_3$ detector accumulated under the condition of γ−β coincidence. (c) Two-dimensional $T \times E$ spectrum, where T is the time between signals from the β- and γ-detectors and E is the amplitude of the signal from γ-detector; time window $\Delta T \approx 20$ ns of γ−β coincidence is outlined. Peaks *1* (1173 keV) and *2* (1332 keV) correspond to the energies of γ-quanta emitted by $^{60}Ni^*$ nuclei; weak background peaks *3–7* are due to registration of the ionizing radiation from radioactive impurities inside the $CeBr_3$ scintillator.

[2] Yu. G. Sobolev, Yu. E. Penionzhkevich, V. V. Samarin, M. A. Naumenko, S. S. Stukalov, I. Siváček, S. A. Krupko, A. Kugler, and J. Louko. Bulletin of the Russian Academy of Sciences: Physics, 2020, Vol. 84, No. 8, pp. 948–956.

Calibration of the γ-spectrometer

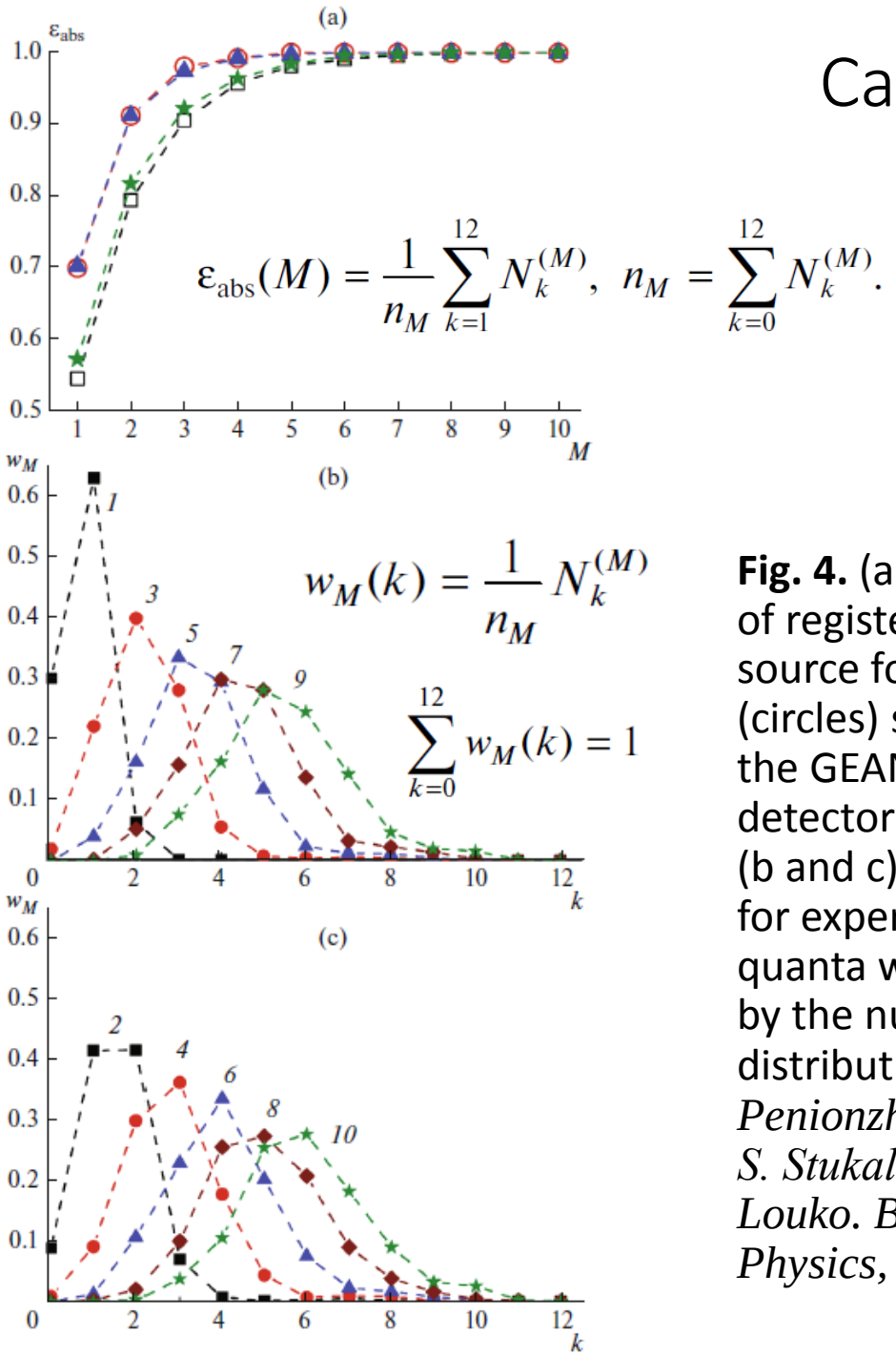

The registration and accumulation of events with multiplicity $M = 1$ and the subsequent combining of records in groups of two, three, or more, allows us to obtain records of simulated events of γ-quantum emission with multiplicities $M = 2$, 3, or more.

We denote the number of the simulated events of emission M γ-quanta in which k spectrometer detectors were triggered as $N_k^{(M)}$, where $k = 0, \ldots, 12$. The absolute efficiency $\varepsilon_{abs}(M)$ for registration of emission events with multiplicity M

Fig. 4. (a) Experimental absolute efficiencies $\varepsilon_{abs}(M)$ of registering γ-cascades, measured with a ^{60}Co source for the 6-detector (squares) and 12-detector (circles) spectrometers, and results simulated using the GEANT-4 code for the 6-detector (stars) and 12-detector (triangles) spectrometers.
(b and c) Probabilities $w_M(k)$ of triggering k detectors for experimentally simulated events of emission of γ-quanta with multiplicity M. The values of M are given by the numbers over the vertices of the distributions. *[2] Yu. G. Sobolev, Yu. E. Penionzhkevich, V. V. Samarin, M. A. Naumenko, S. S. Stukalov, I. Siváček, S. A. Krupko, A. Kugler, and J. Louko. Bulletin of the Russian Academy of Sciences: Physics, 2020, Vol. 84, No. 8, pp. 948–956.*

Experiment: identification of beam nuclei

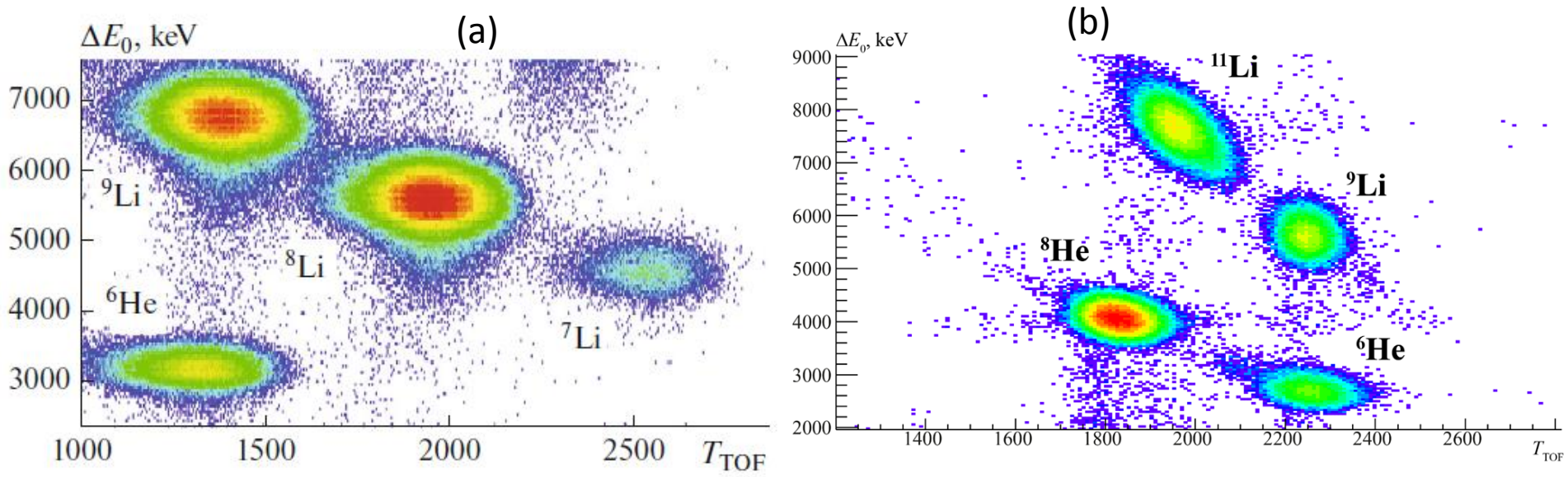

Fig. 5. Two-dimensional $T_{TOF} \times \Delta E_0$ spectrum for identification of beams of ^{6}He and ^{7,8,9}Li nuclei (a), ^{6,8}He and ^{9,11}Li nuclei (b) in front of a target. The time of flight (in the channels) is plotted on the abscissa axis. The energy losses of beam particles in a 243-μm thick ΔE_0 detector are plotted on the ordinate axis. The statistics for the ^{7}Li nuclei are considerably lower than those for the rest of the nuclei. [2]

[2] *Yu. G. Sobolev, Yu. E. Penionzhkevich, V. V. Samarin, M. A. Naumenko, S. S. Stukalov, I. Siváček, S. A. Krupko, A. Kugler, and J. Louko. Bulletin of the Russian Academy of Sciences: Physics, 2020, Vol. 84, No. 8, pp. 948–956.*

Results of experiments: background

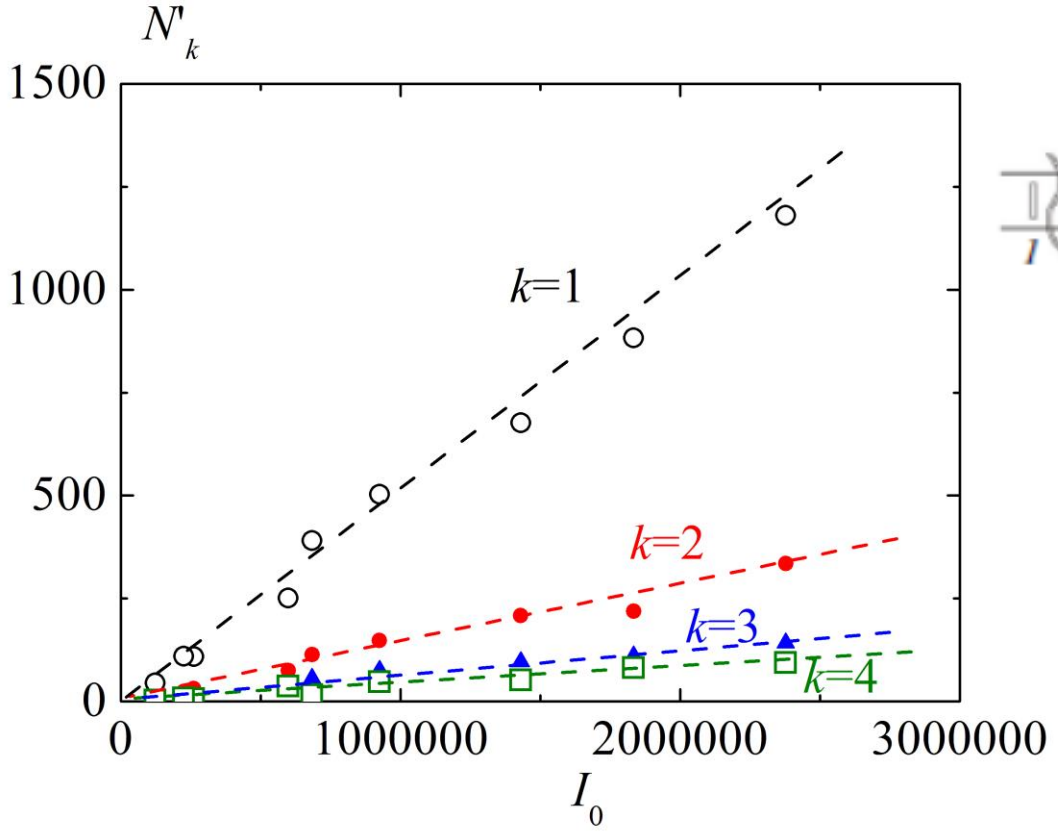

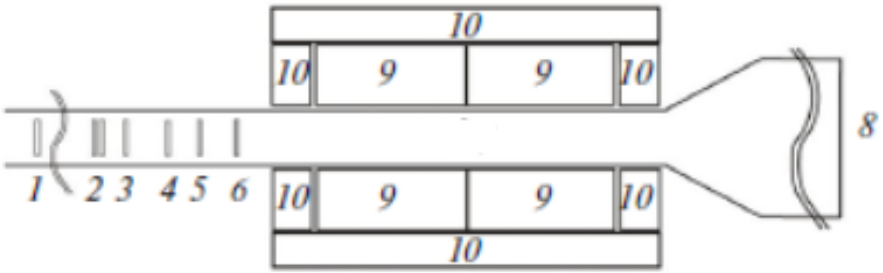

Fig. 6. N'_k are the numbers of the reaction events with triggering of k detectors without the target. The ratio between number N'_k with number I_0 of particles flown into the spectrometer was approximated by the linear dependence $N'_k = \beta_k I_0$ with background coefficients β_k determined using the least squares method from the results of m measurements. The values of error $\delta\beta_k$ were estimated via linear regression.

Results of experiments: the numbers of the reaction events with triggering of *k* detectors

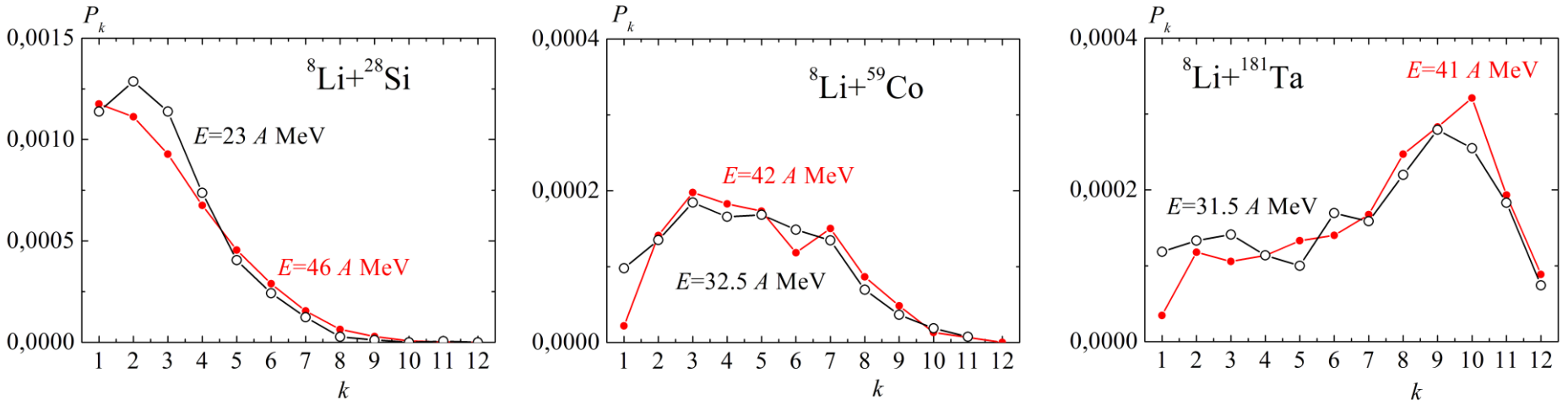

Fig. 7. Values of relative frequencies of the number of the detected events with the background subtracted for the reactions of ^{8}Li nuclei on ^{28}Si, ^{59}Co, and ^{181}Ta targets $P_k=N_k/I_0-\beta_k$, here N_k are the numbers of the reaction events with triggering of k detectors with the target.

Results of experiments: the numbers of the reaction events with triggering of *k* detectors

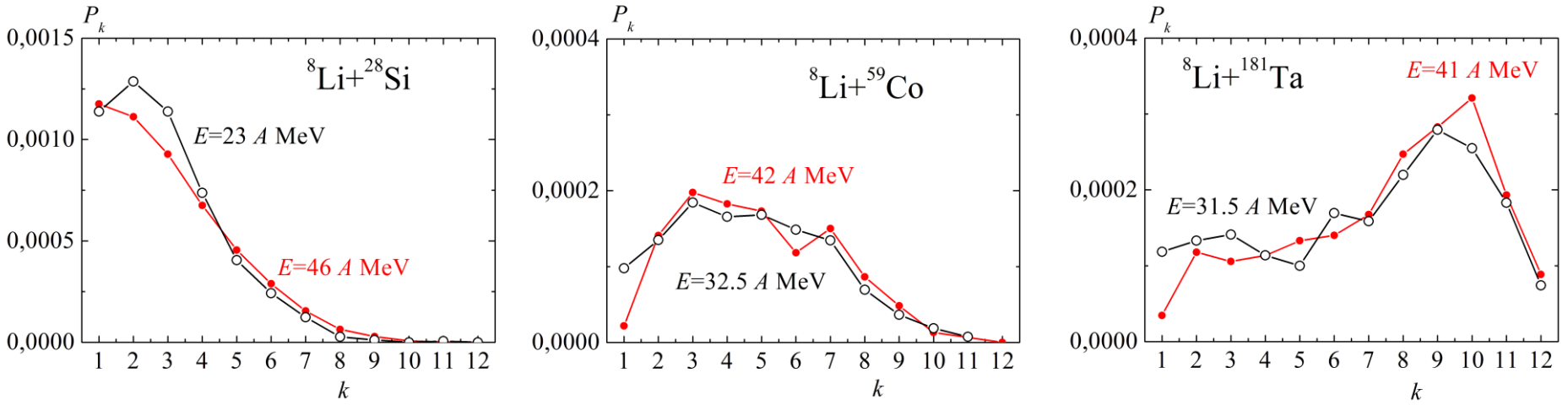

Fig. 7. Values of relative frequencies of the number of the detected events with the background subtracted for the reactions of ^{8}Li nuclei on ^{28}Si, ^{59}Co, and ^{181}Ta targets $P_k=N_k/I_0-\beta_k$, here N_k are the numbers of the reaction events with triggering of *k* detectors with the target.

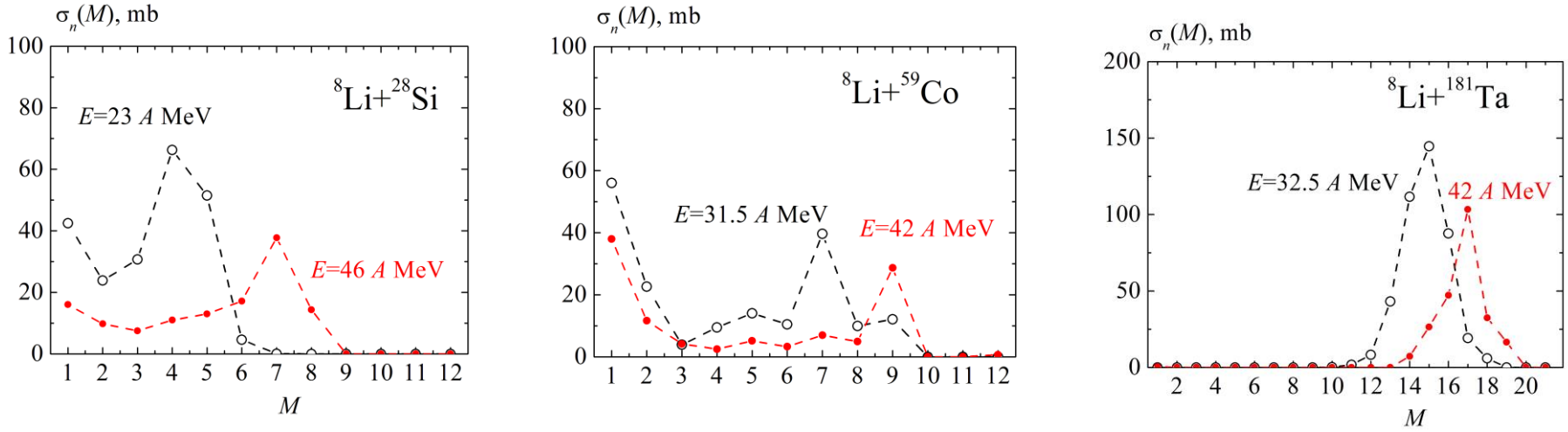

Fig. 8. Values of cross sections of emission of M neutrons, results of fusion-evaporation calculations using NRV knowledge base **http://nrv.jinr.ru**

Scheme of the data processing

Let N_k and N_k' be the numbers of the reaction events with triggering of k detectors with and without the target, respectively. When the measurements were made without the target, the ratio between number N_k' of triggering of k detectors with number I_0 was approximated by the linear dependence

$$N_k' = \beta_k I_0 \qquad \beta_k = \frac{\sum_{j=1}^{m} I_{0j} N_{kj}'}{\sum_{j=1}^{m} I_{0j}^2}.$$

with background coefficients β_k determined using the least squares method from the results of m measurements. The values of error $\delta\beta_k$ were estimated via linear regression .

The measured reaction cross section taking into account the number k of the triggered detectors of the segmented spectrometer was found as described below. Let M γ-quanta (and/or neutrons) be emitted in every reaction event with probability $\Gamma(M)$, $1 \le M \le M_{\max}$, then the probability of triggering of k detectors when registering a reaction is

$$P(k) = \sum_{M=1}^{M_{\max}} \Gamma(M) w_M(k). \qquad (11)$$

For total number of reactions $I_R = I_0 \sigma_R n d$, the calculated number of their registrations with triggering of k detectors is

$$P(k) I_R = \eta I_0 \sigma_R n d \sum_{M=1}^{M_{\max}} \Gamma(M) w_M(k). \qquad (12)$$

Here, η is a correction for nonisotropic neutron emission in the forward direction upon the breakup of weakly bound ^{8}Li and ^{8}He nuclei.

From the condition of the equality of the number of registered events to their calculated value $N_k - N_k' = N_k - \beta_k I_0$, we obtain the system of linear equations for unknowns $\tilde{\sigma}_M = \eta\sigma_M = \eta\sigma_R\Gamma(M)$:

$$\sum_{M=1}^{M_{\max}} \tilde{\sigma}_M w_M(k) - \frac{N_k - \beta_k I_0}{I_0 n d} = 0.$$

Since the coefficients of system (13) were determined with errors, the exact solution for the system could produce nonphysical values of $\tilde{\sigma}_M < 0$. It would therefore be more correct to find the unknown values of $\tilde{\sigma}_M$ from the condition of the minimum for the sum of squares of the left-hand sides:

$$F(\tilde{\sigma}_1, \ldots, \tilde{\sigma}_{M_{\max}}) = \sum_{k=1}^{12} \left[\sum_{M=1}^{M_{\max}} \tilde{\sigma}_M w_M(k) - \frac{N_k - \beta_k I_0}{I_0 n d} \right]^2$$

under constraint $\tilde{\sigma}_M \ge 0$.

Total reaction cross section σ_R is determined using the formula

$$\sigma_R = \frac{\tilde{\sigma}_R}{\eta}, \quad \tilde{\sigma}_R = \sum_{M=1}^{M_{\max}} \tilde{\sigma}_M.$$

Errors $\delta\beta_k$ of coefficients β_k lead to error $\Delta\tilde{\sigma}_R$ of the quantity $\tilde{\sigma}_R$. The value of $\Delta\tilde{\sigma}_R$ can be estimated using the formula $\Delta\tilde{\sigma}_R = \max\left\{\left|\tilde{\sigma}_R^{(+)} - \tilde{\sigma}_R\right|, \left|\tilde{\sigma}_R^{(-)} - \tilde{\sigma}_R\right|\right\}$, where $\tilde{\sigma}_R^{(+)}$ and $\tilde{\sigma}_R^{(-)}$ are the values obtained for set of parameters $\beta_k + \delta\beta_k$ and $\beta_k - \delta\beta_k$, respectively. The relative ε_σ and absolute $\Delta\sigma_R$ errors of the total reaction cross section were estimated using the expressions

$$\varepsilon_\sigma = \frac{\Delta\tilde{\sigma}_R}{\tilde{\sigma}_R} + \frac{\Delta\eta}{\eta}, \quad \Delta\sigma_R = \sigma_R \varepsilon_\sigma.$$

Energy dependences of total reaction cross sections

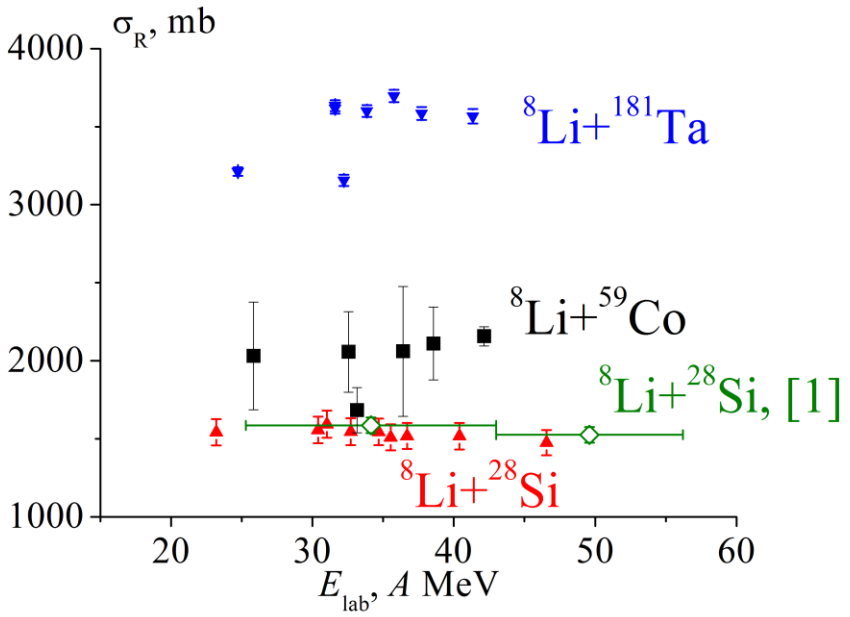

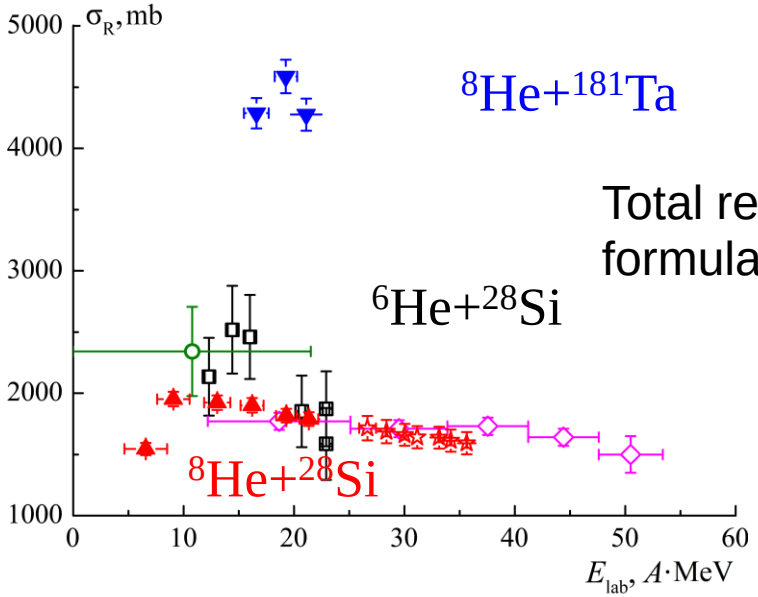

Fig. 9. (a) Total cross sections of reactions ^{8}Li + ^{28}Si (upright triangles), ^{8}Li + ^{59}Co (squares), and ^{8}Li +^{181}Ta (inverted triangles) obtained in this work , compared to total cross section of the ^{8}Li + ^{28}Si reaction obtained in [1] (diamonds). [1] R. E. Warner et al. Phys. Rev. C V. 54, p. 1700 (1996).
(b) Total cross sections of the reactions of ^{8}He nuclei on ^{28}Si (upright triangles and ^{181}Ta (inverted triangles) targets obtained in this work, compared to the total cross section of the ^{6}He + ^{28}Si reaction obtained in [2] (empty squares), [1] (diamonds), [3] (circle), and [4, 5] (stars).

[2] Sobolev, Yu.G., Penionzhkevich, Yu.E., Maslov, V.A., et al., *Bull. Russ. Aca Sci.: Phys.*, 2019, vol. 83, p. 402.
[3] Villari, A.C.C., Mittig, W., Plagnol, E., et al., *Phys. Lett. B*, 1991, vol. 268, p
[4] Saint-Laurent, M.G., Anne, R., Bazin, D., et al., *Z. Phys. A*, 1989, vol. 332,
[5] Li, Ch., Zhan, W-L., Xiao, G-Q., et al., *High Energy Phys. Nucl. Phys.*, 200 vol. 31, no. 1, p. 52.

Total reaction cross section is determined using the formula

$$\sigma_R = \frac{\tilde{\sigma}_R}{\eta},\ \tilde{\sigma}_R = \sum_{M=1}^{M_{max}} \tilde{\sigma}_M$$

Here, η is a correction for nonisotropic neutron emission in the forward direction upon the breakup of weakly bound ^{8}Li and ^{8}He nuclei. This correction was found under the assumption that it depends mainly on the energy of separation of one or two external neutrons. To find the values of , the total cross sections of the reactions with the ^{8}Li, ^{8}He and ^{6}He nuclei were

Energy dependences of total reaction cross sections

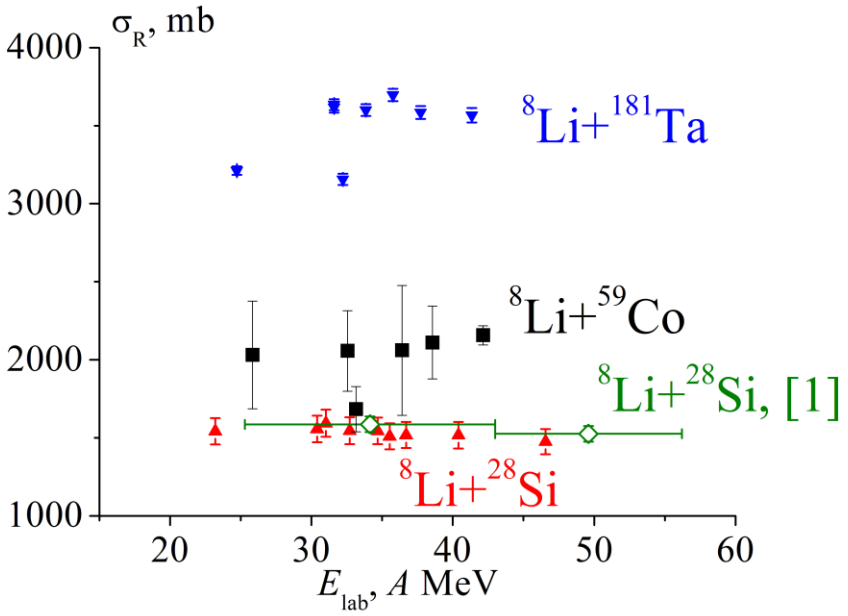

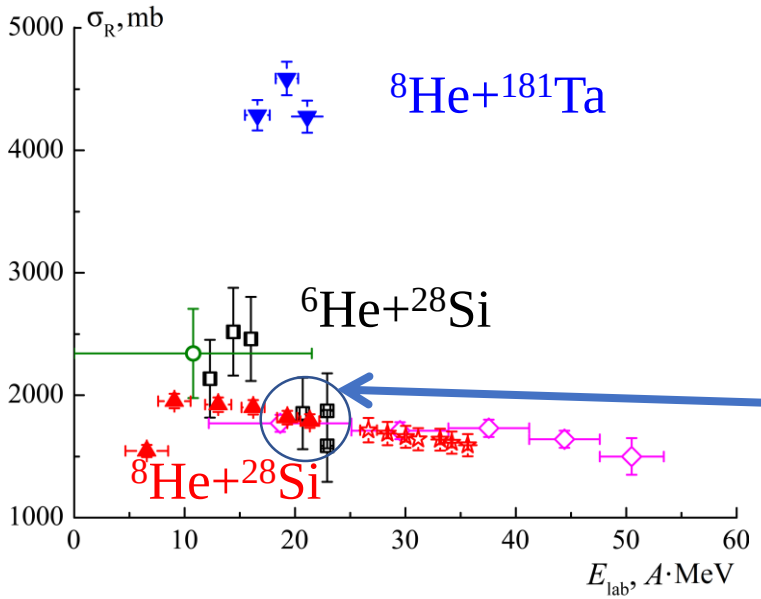

The total reaction cross sections of ^{8}Li nuclei on ^{59}Co and ^{181}Ta targets exceed those of the ^{8}Li + ^{28}Si reaction by around 1.5 and 2.2 times, respectively. The ratio of the cross sections for fusion reactions of ^{8}Li nuclei with stable heavy nuclei with mass numbers A_1 and A_2 is approximately equal to the ratio of the geometric cross sections of these nuclei, which can be estimated as $\left[\left(8^{1/3}+A_1^{1/3}\right)/\left(8^{1/3}+A_2^{1/3}\right)\right]^2$

For the pairs of nuclei ^{59}Co–^{28}Si and ^{181}Ta –^{28}Si, these ratios are 1.37 and 2.31, respectively, which is close to the experimental values. The total reaction cross section can be approximated as the sum of the fusion cross section and the cross section of peripheral reactions, the ratio of the latter can be estimated as $\left[\left(9^{1/3}+A_1^{1/3}\right)/\left(9^{1/3}+A_2^{1/3}\right)\right]$

For the pairs of nuclei ^{59}Co–^{28}Si and ^{181}Ta –^{28}Si, these –$_{28}$Si and $_{181}$Ta–$_{28}$Si, these ratio are 1.17 and 1.52, respectively. On the whole, the above)btained total cross sections of ^{8}Li, ^{8}He + ^{28}Si,

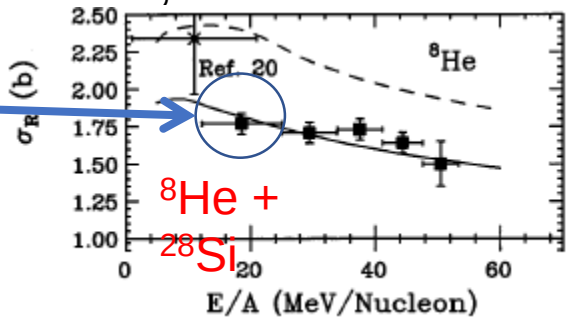

R. E. Warner et al. Phys. Rev. C V. 54, p. 1700 (1996).

Properties of He и Li isotopes

The correction η was found under the assumption that it depends mainly on the energy of separation of one or two external neutrons, for ^{8}Li, ^{8}He η=0.9 and for ^{6}He η=0.83.

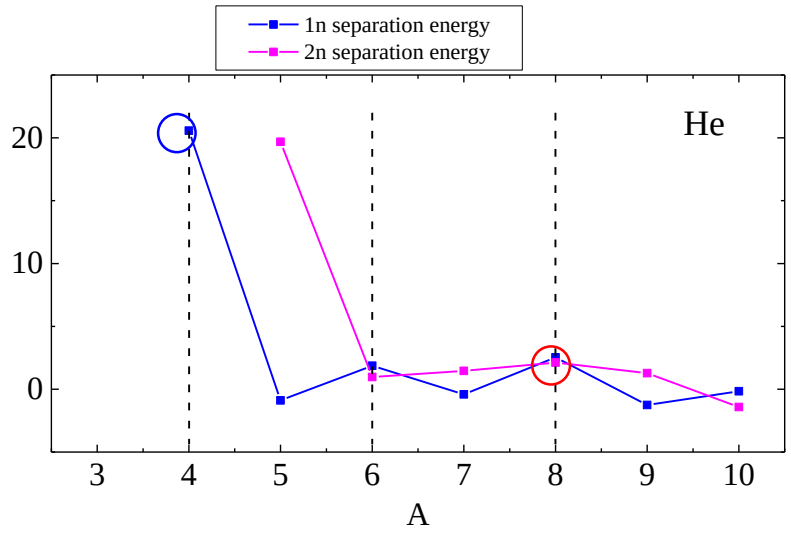

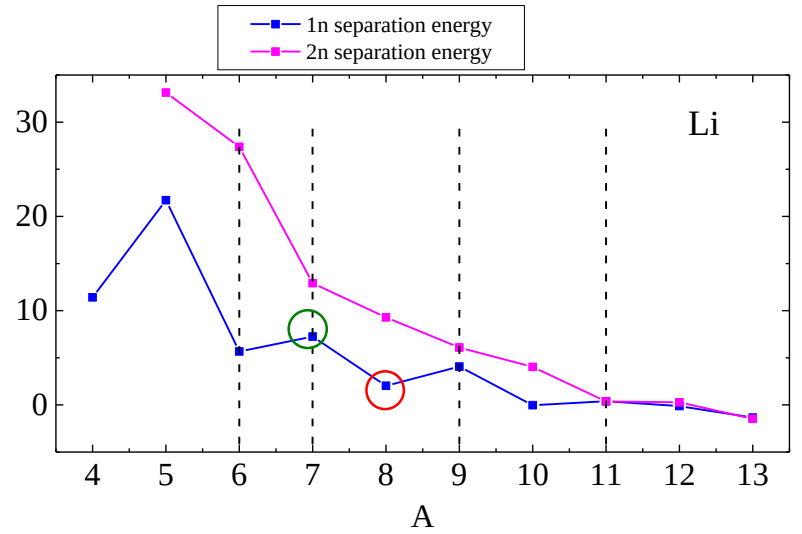

Fig. 10.

^{8}He (α + *n* + *n* + *n* + *n*)

- J(π)=0+
- Binding energy (MeV) 31.396
- Binding energy (MeV/A) 3.925
- Separation energy: 1n (MeV) 2.53475
- Separation energy: 2n (MeV) 2.12501
- Separation energy: 1p (MeV) 24.81432
- Charge radius (fm) 1.9239 ± 0.0306 [1]

^{8}Li ({^{7}Li } + *n*)

- J(π)=2+
- Binding energy (MeV) 41.278
- Binding energy (MeV/A) 5.160
- Separation energy: 1n (MeV) 2.03260
- Separation energy: 2n (MeV) 9.28367
- Separation energy: 1p (MeV) 12.41632
- Separation energy: 2p (MeV) 35.50791
- Separation energy: α (MeV) 6.10022
- Charge radius (fm) 2.339 ± 0.044 [1]

http://nrv.jinr.ru

NRV knowledge base http://nrv.jinr.ru

The NRV web knowledge base is a unique interactive research system:

- Allows to run complicated computational codes
- Works in any internet browser supporting Java plugin
- Has graphical interface for preparation of input parameters and analys
- Combines computational codes with experimental databases on prope reactions
- Contains detailed description of models

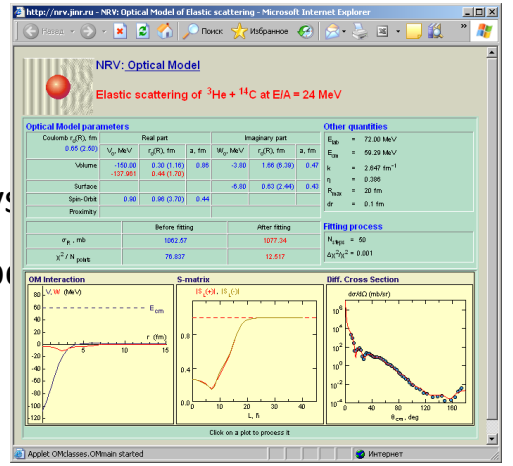

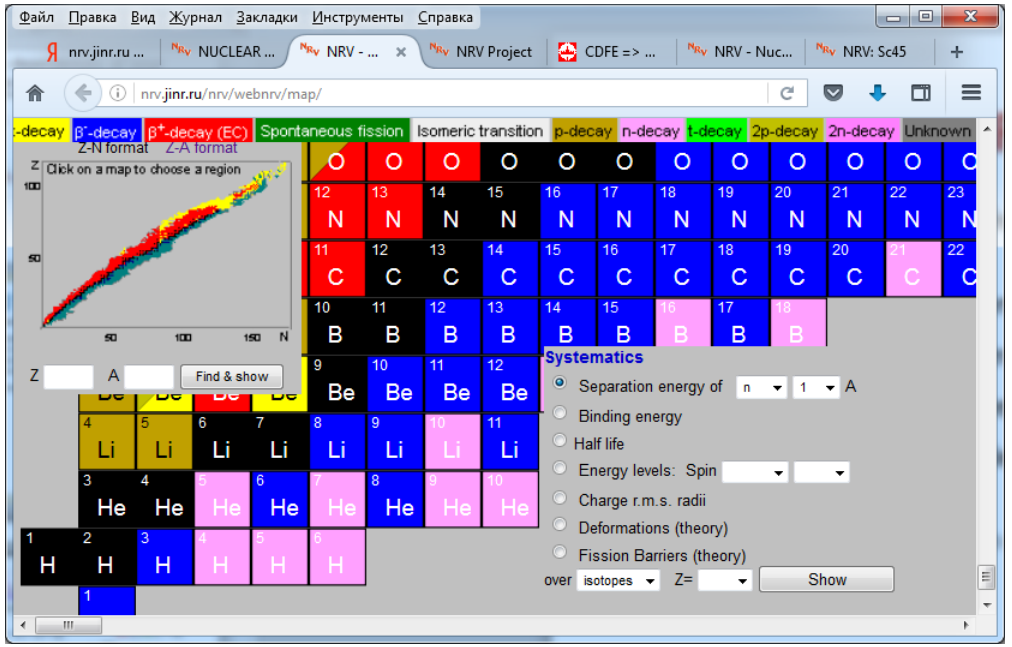

Structure of projectile nuclei ^{8}Li, ^{8}He

Projectile nuclei ^{8}Li and ^{7}Liwere nonspherical. The experimental absolute values of quadrupole deformation $|\beta_2|$ for the first nucleus were 0.542 ± 0.033, 0.476 ± 0.075, and 0.526 ± 0.054 [19].

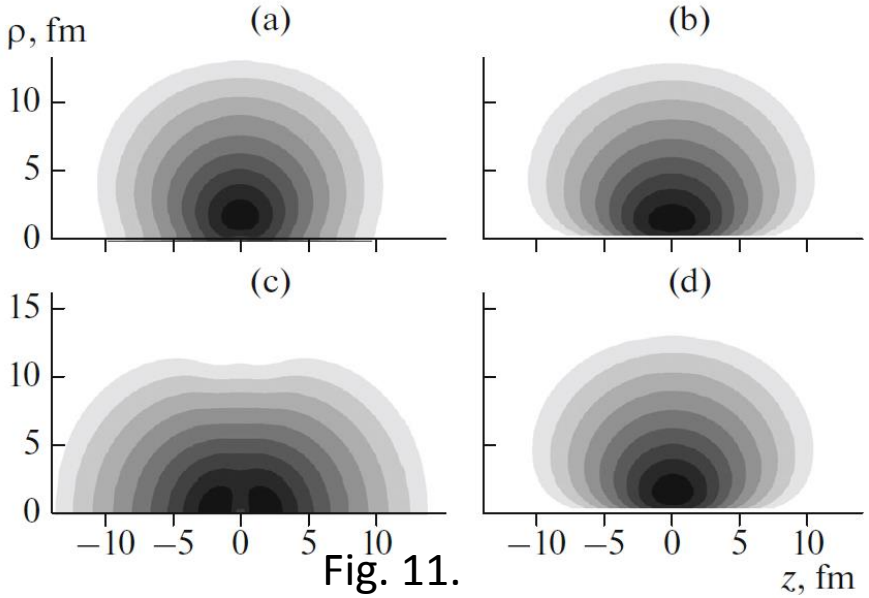

Fig. 11.

Fig. 1. Probability densities in the cylindrical coordinate system for the outer neutron of ^{8}Li on the values of the deformation parameters: (a) $\beta_2 = -0.5$, (b) $\beta_2 = 0.5$, and (c, d) $\beta_2 = 0$. The absolute values of the total angular momentum projection on the axis of symmetry z of the deformed nucleus are (a) $|m_j| = 1/2$, (b) $|m_j| = 3/2$, (c) $|m_j| = 1/2$, and (d) $|m_j| = 3/2$.

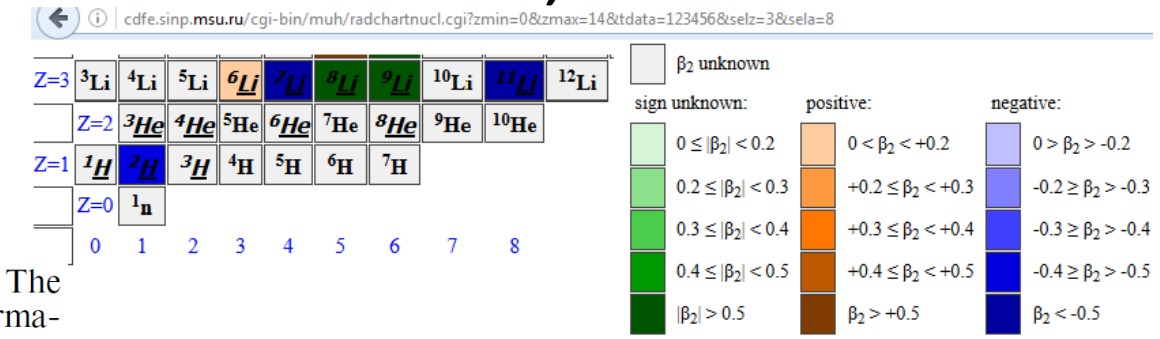

19. Chart of nucleus shape and size parameters. http://cdfe.sinp.msu.ru/services/radchart/radmain.html.

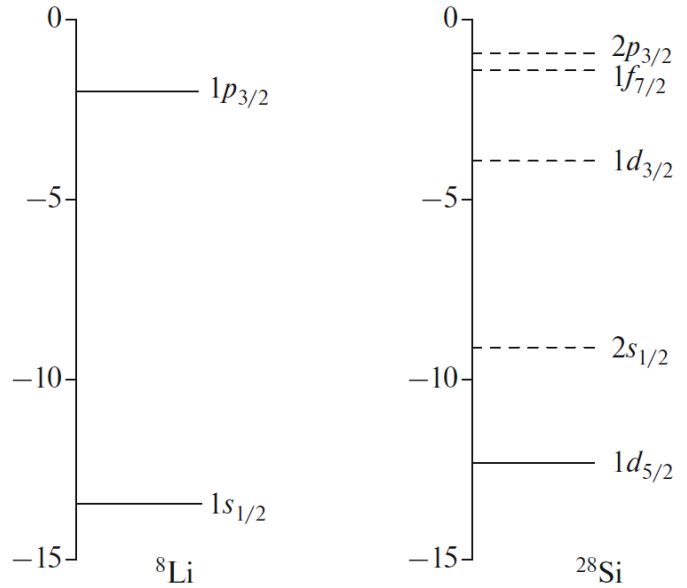

Fig. 12.

Energy level diagram of neutron of the projectile nuclei ^{8}Li, ^{8}He and target nucleus ^{28}Si in the shell model of a spherical nucleus.

Time-dependent Schrödinger equation approach

- Classical motion of centers of nuclear cores

$$m_1\ddot{\vec{r}}_1 = -\nabla_{\vec{r}_1} V_{12}\left(\left|\vec{r}_1 - \vec{r}_2\right|\right),\ m_2\ddot{\vec{r}}_2 = -\nabla_{\vec{r}_2} V_{12}\left(\left|\vec{r}_2 - \vec{r}_1\right|\right).$$

- Transfer (rearrangement) of neutrons during collision is described by time-dependent Schrödinger equation with spin-orbit interaction [1-4]

$$i\hbar\frac{\partial}{\partial t}\Psi(\vec{r},t) = \left\{-\frac{\hbar^2}{2m}\Delta + V_1(\left|\vec{r}-\vec{r}_1(t)\right|) + V_2(\left|\vec{r}-\vec{r}_2(t)\right|) + \hat{V}_{LS}^{(1)}\left(\vec{r}-\vec{r}_1(t)\right) + \hat{V}_{LS}^{(2)}\left(\vec{r}-\vec{r}_2(t)\right)\right\}\Psi(\vec{r},t),$$

$$\Psi = \begin{pmatrix}\psi_1(\vec{r},t)\\ \psi_2(\vec{r},t)\end{pmatrix},\quad \hat{V}_{LS}^{(i)} = -\lambda_i\frac{\hbar}{(2mc)^2}\vec{\sigma}\left[\nabla V_i\hat{\vec{p}}\right].$$

- The initial wave function is determined from shell model. Parameters of shell model were chosen based on experimental data on charge radii and neutron separation energies.

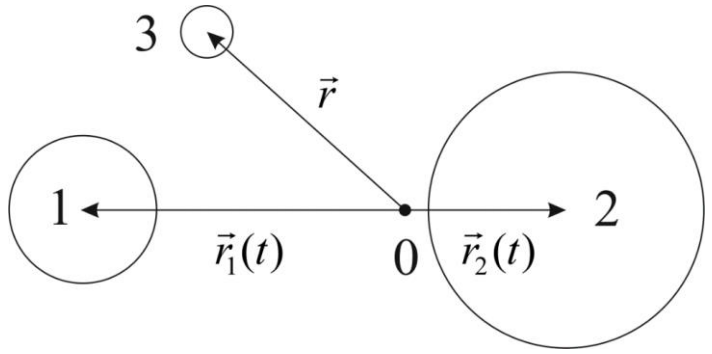

1,2 are two heavy classical particles (nuclear cores); 3 is light quantum particle (neutron of projectile or target).

References

[1] V. V. Samarin, EPJ Web Conf. **66**, 03075 (2014); **86**, 00040 (2015).

[2] V. V. Samarin. Phys. At. Nucl. **78**,128 (2015).

[3] M. A. Naumenko, V. V. Samarin, Yu. E. Penionzhkevich, N. K. Skobelev. Bull. Russ. Acad. Sci. Phys. **80**, 264 (2016).

[4] M. A. Naumenko, V. V. Samarin, Yu. E. Penionzhkevich, N. K. Skobelev. Bull. Russ. Acad. Sci. Phys. **81**, 710 (2017).

Some theoretical approaches to description of neutron transfer

- **Time-dependent Schrödinger equation (TDSE):**
  - the quantum description of several independent external neutrons,
  - a small 3D grid step (0.1 - 0.2 fm, smaller than the length of the probability density oscillations),
  - the classical description of the motion of the centers of nuclei,
  - may be used for light nuclei,
  - quick calculation.

These methods have shortcomings:

- **Time-dependent Hartree-Fock (TDHF):**
  - self-consistent quantum motion of all nucleons,
  - averaged over a large grid step (0.8 fm), exceeding the length of the oscillations of the probability density for the individual states,
  - used for heavy and medium-mass nuclei only,
  - long calculation.

- **Langevin equations:**
  - equations of classical mechanics with stochastic forces together including mass asymmetry degrees of freedom,
  - used for heavy and medium-mass nuclei,
  - no quantum description of the individual nucleons.

- **Distorted wave Born approximation (DWBA):**
  - calculation of the differential cross section for specific channels,
  - takes into account the explicit form of the wave functions of the initial and the final collective or single-particle states (within the perturbation theory) using phenomenological optical nucleus-nucleus potentials,
  - does not provide a dynamic picture.

Benefits of time-dependent Schrödinger equation approach

- quantum description of several independent external neutrons,
- small 3D mesh step (0.1 - 0.2 fm, smaller than the length of the probability density oscillations),
- classical description of the motion of centers of nuclei,
- may be used for light nuclei,
- fast calculation,
- **intuitive visualization of dynamics.**

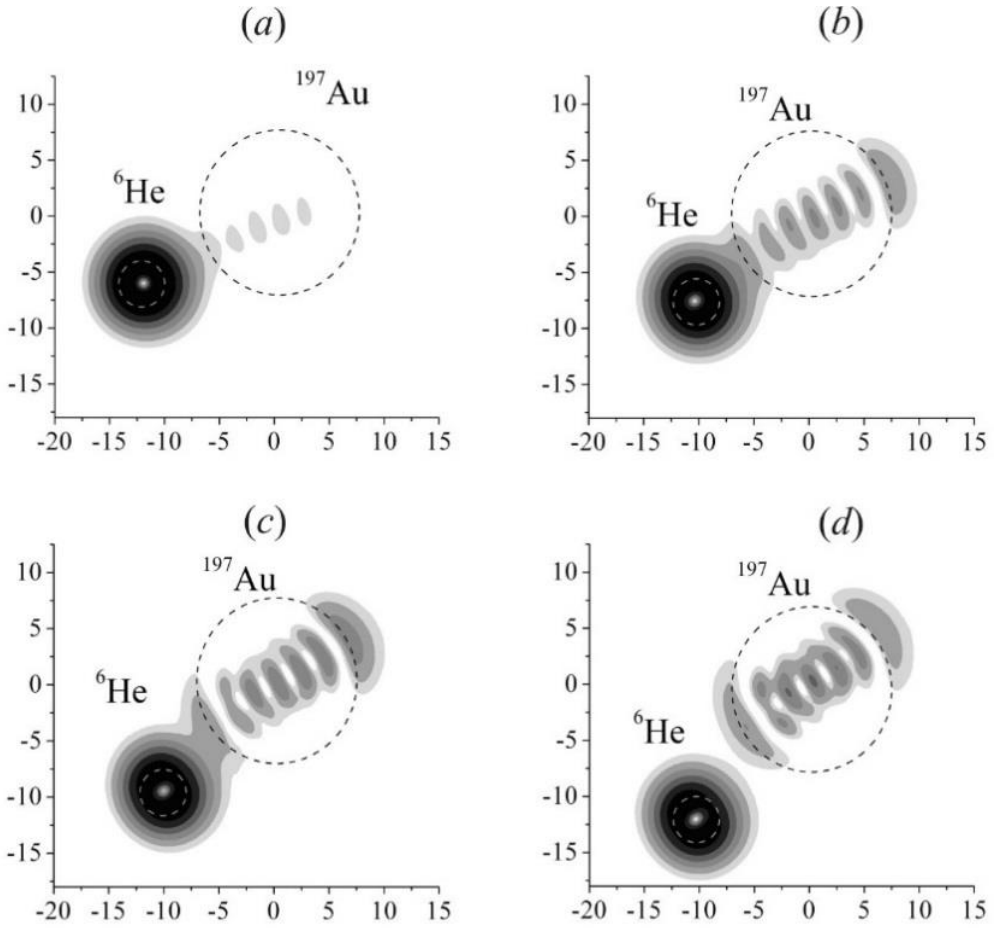

Fig. 13.

The change in the probability density and the rearrangement of the valence neutron of the ^{6}He nucleus during a collision with the ^{197}Au nucleus at E_{cm}= 19 MeV, b =4 fm. The course of time corresponds to panels (*a*) - (*d*). The mesh spacing is 0.2 fm.

Time-dependent Schrödinger equation approach for transfer and break up channels

$$\rho(\vec{r},t)=\frac{1}{4}\sum_{m_j=-3/2}^{3/2}\left[\left|\psi_{m_j}(\vec{r},t)\right|^2+\left|\varphi_{m_j}(\vec{r},t)\right|^2\right] \qquad \Psi_{m_j}(\vec{r},t=0)=\begin{pmatrix}\psi_{1,1,3/2,m_j}(\vec{r})\\ \varphi_{1,1,3/2,m_j}(\vec{r})\end{pmatrix}.$$

Fig. 14.

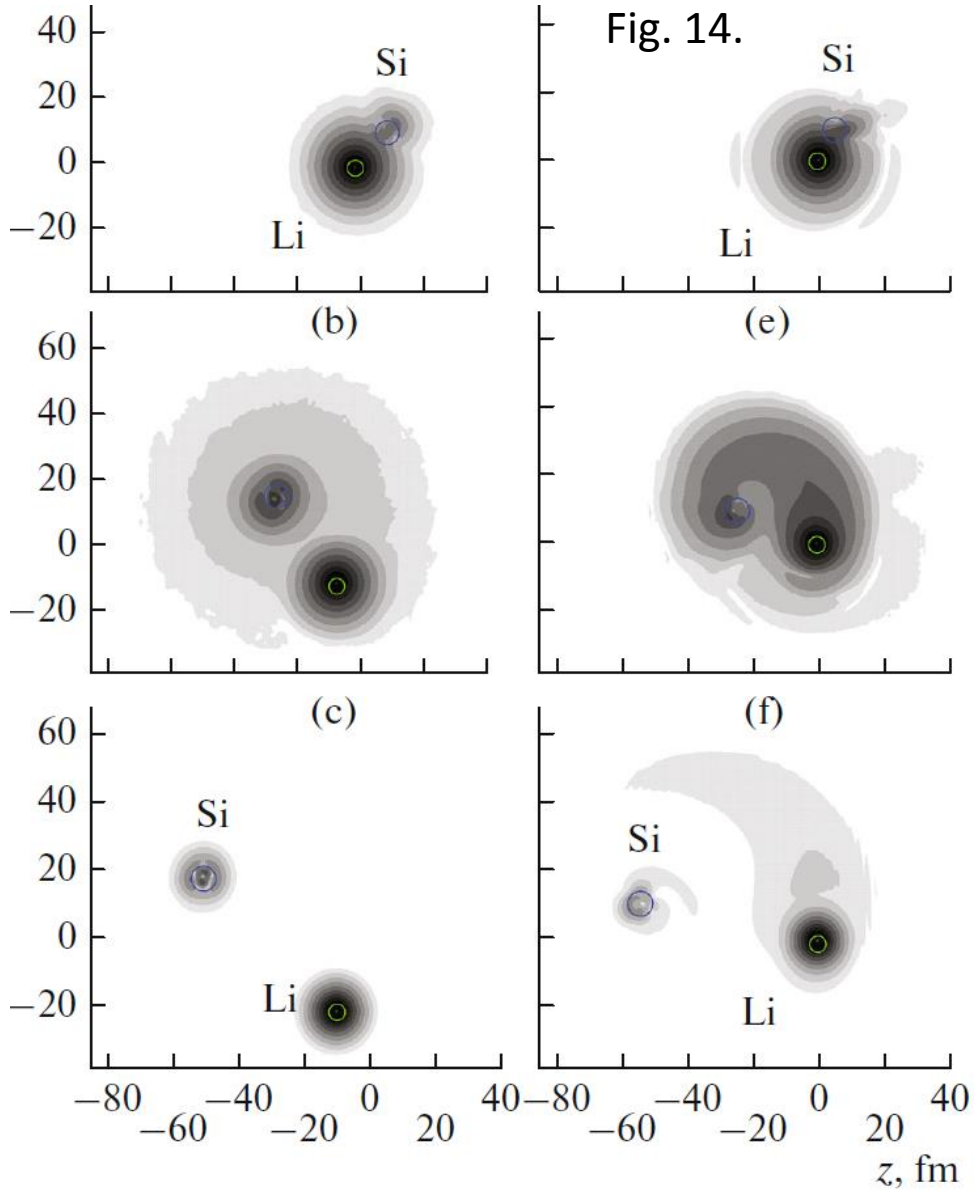

In this work, we perform a numerical solving of Eq. (2) in a system moving with respect to the laboratory system with constant velocity equal to that of a projectile nucleus at a fair distance from the target nucleus, due to the large extension of nucleon clouds in ^{8}Li and ^{8}B. This allows us to reduce the mesh size and shorten the time needed for calculations.

In our calculations, the mesh size was $h = 0.3$ fm, and the typical volume of the region was 8×10^5 fm^3 for a mesh of $220 \times 360 \times 380$ cells with the largest number of nodes in the collision plane. Calculations of the process of nuclei collision required several thousand time steps.

Fig. 3. Evolution of the probability density for an outer neutron of ^{8}Li with initial state $1p_{3/2}$ in collision ^{8}Li + ^{28}Si (a, b, c) for $E_{\text{c.m.}} = 10$ MeV, $E_{\text{lab}} = 1.6$ MeV/nucleon, along with impact parameter $b = 10$ fm and (d, e, f) for $E_{\text{c.m.}} = 186$ MeV, $E_{\text{lab}} = 30$ MeV/nucleon, $b = 9$ fm in a reference system moving relative to the laboratory system with a constant velocity equal to that of a projectile at a fairly large distance from the target nucleus. Time runs top-down. Greyscale gradation in the logarithmic scale corresponds to ranges (a, b, d, e) from 5×10^{-10} to 0.008 and (c, f) from 2×10^{-7} to 0.008. The radii of the circles correspond to those of nuclear cores of 2.4 fm and 3.8 fm, respectively.

Probabilities of the neutron loss and transfer

The amplitude of the probability for the nucleon to remain in initial state $1p_{3/2}$ of the projectile nucleus at time t is

$$c(t) = \sum_{n_j=-3/2}^{3/2} \frac{1}{4} \times \sum_{m_j=3/2}^{3/2} \int \left[\tilde{\psi}^{(0)*}_{n_j}(\vec{r},t)\psi_{m_j}(\vec{r},t) + \tilde{\varphi}^{(0)*}_{n_j}(\vec{r},t)\varphi_{m_j}(\vec{r},t) \right] dV, \quad (9)$$

where the wave function of state $1p_{3/2}$ with the projection of total momentum m_j in a projectile nucleus moving with slowly varying velocity $\vec{v}_1(t)$ is

$$\tilde{\Psi}^{(0)}_{m_j}(\vec{r},t) = \begin{pmatrix} \tilde{\psi}^{(0)}_{m_j}(\vec{r},t) \\ \varphi^{(0)}_{m_j}(\vec{r},t) \end{pmatrix} = \begin{pmatrix} \psi^{(0)}_{m_j}(\vec{r} - \vec{r}_1(t)) \\ \varphi^{(0)}_{m_j}(\vec{r} - \vec{r}_1(t)) \end{pmatrix} \exp\left(i\hbar^{-1} m \vec{v}_1(t)\vec{r} \right). \quad (10)$$

Total probability P_{loss} of neutron loss by the projectile nucleus can be determined as a reduction in the population of the state $1p_{3/2}$

$$P_{\text{tr}}(t) = \sum_k |a_k(t)|^2, \; P_{\text{loss}}(t) = 1 - |c(t)|^2 \quad (11)$$

$$a_k(t) = \int \left[\tilde{\psi}^*_k(\vec{r},t)\psi(\vec{r},t) + \tilde{\varphi}^*_k(\vec{r},t)\varphi(\vec{r},t) \right] dV$$

The wave function of the k-th bound state in a target nucleus moving after colliding with slowly varying velocity $\vec{v}_2(t)$ is

$$\tilde{\Psi}_k(\vec{r},t) = \begin{pmatrix} \tilde{\psi}_k(\vec{r},t) \\ \tilde{\varphi}_k(\vec{r},t) \end{pmatrix} = \begin{pmatrix} \psi_k(\vec{r} - \vec{r}_2(t)) \\ \varphi_k(\vec{r} - \vec{r}_2(t)) \end{pmatrix} \exp\left(i\hbar^{-1} m \vec{v}_2(t)\vec{r} \right).$$

Fig. 15.

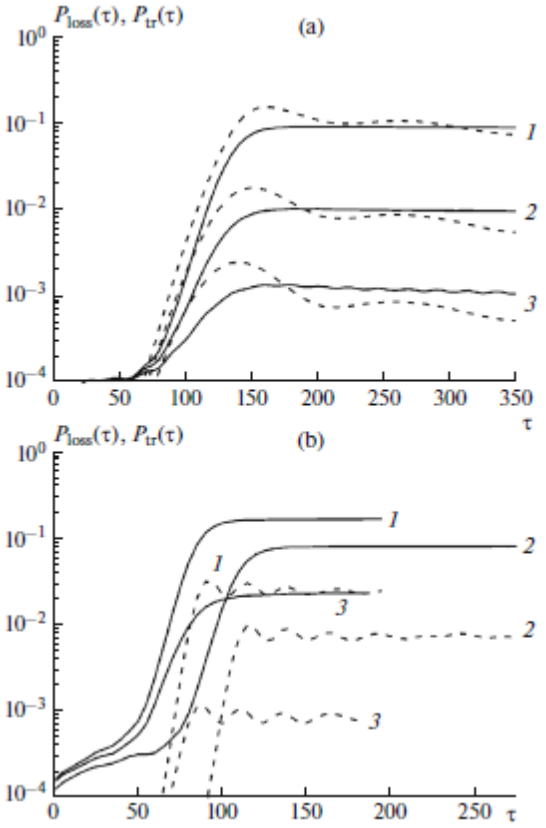

Fig. 5. (Solid curves) $P_{\text{loss}}(\tau)$ and (dashed curves) $P_{\text{tr}}(\tau)$ as functions of dimensionless time $\tau = t/t_0$, $t_0 = 1.57 \times 10^{-23}$ s for collisions (a) ^{8}Li + ^{28}Si and (b) ^{8}B + ^{28}Si, energies (a) $E_{\text{c.m.}} = 10$ MeV, $E_{\text{lab}} = 1.6$ MeV/nucleon and (b) $E_{\text{c.m.}} = 25$ MeV, $E_{\text{lab}} = 4$ MeV/nucleon, and impact parameters (a) $b = 7$ fm (curves *1*), $b = 10$ fm (curves *2*), $b = 13$ fm (curves *3*); (b) $b = 7$ fm (curves *1*), $b = 8$ fm (curves *2*), $b = 10$ fm (curves *3*).

Calculations of the neutron loss and transfer cross sections

$$\sigma_{\text{loss}}(E) = 2\pi \int_{b_{\min}}^{\infty} p_{\text{loss}}(b,E)\left[1 - f(R_{\min})\right] b\,db, \quad (17)$$

$$\sigma_{\text{tr}}(E) = 2\pi \int_{b_{\min}}^{\infty} p_{\text{tr}}(b,E)\left[1 - f(R_{\min})\right] b\,db, \quad (18)$$

$$p_{\text{tr}}(b,E) = \min\left\{\tilde{P}_{\text{tr}}(R_{\min}(b,E)),1\right\}, \quad (19)$$

$$p_{\text{tr}}(b,E) = \min\left\{\tilde{P}_{\text{tr}}(R_{\min}(b,E)),1\right\}. \quad (20)$$

$$f(R_{\min}) = \frac{1}{1 + \exp\left(\dfrac{R_{\min} - R_{\text{f}}}{a_{\text{f}}}\right)}$$

Fig. 16.

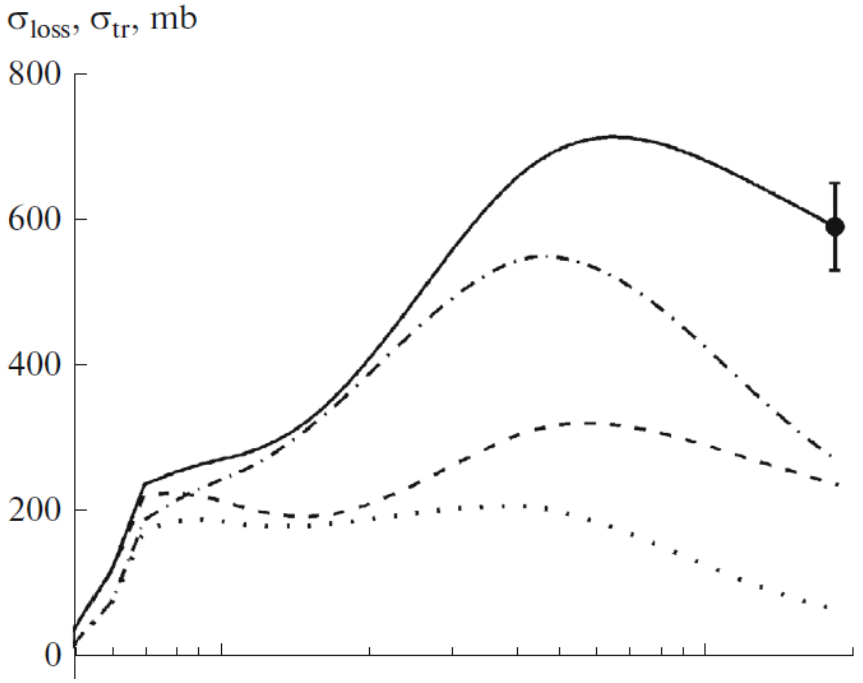

Fig. 7. Calculated loss cross section $\sigma_{\text{loss}}(E_{\text{c.m.}})$ and transfer cross section $\sigma_{\text{tr}}(E_{\text{c.m.}})$ for outer neutron of ^{8}Li in reaction ^{8}Li + ^{28}Si for two values of the average fusion radius of nuclei R_{f}: R_{f} = 7 fm (dashed curves) $\sigma_{\text{loss}}(E_{\text{c.m.}})$, (dotted curves) $\sigma_{\text{tr}}(E_{\text{c.m.}})$, and R_{f} = 4.9 fm (solid curves) $\sigma_{\text{loss}}(E_{\text{c.m.}})$, (dashed-and-dotted curves) $\sigma_{\text{tr}}(E_{\text{c.m.}})$. The experimental point is the value of $\sigma_{\text{loss}}(E_{\text{c.m.}})$ for ^{8}Li + ^{28}Si in [7].

We used approximations:

the natural set of parameters

$$R_{\text{f}} \approx \frac{1}{2}(R_{\text{cont}} + R_{\text{B}}), \quad a_{\text{f}} \approx \frac{1}{2}(R_{\text{B}} - R_{\text{cont}})$$

$$R_{\text{f}} = 7 \text{ fm}, \; a_{\text{f}} = 1 \text{ fm}. \quad R_{\text{cont}} = R_1 + R_2$$

$$P_{\text{tr}} \approx \tilde{P}_{\text{tr}}(R_{\min}) = \exp(A_{\text{tr}} - B_{\text{tr}} R_{\min}).$$

$$P_{\text{loss}} \approx \tilde{P}_{\text{loss}}(R_{\min}) = \exp(A_{\text{loss}} - B_{\text{loss}} R_{\min})$$

Conclusions

- The distributions over the number of triggered detectors of a segmented γ-spectrometer were measured and used for obtaining of total reaction cross sections for ^{8}Li, ^{8}He + ^{28}Si, ^{8}Li, ^{8}He + ^{59}Co, ^{8}Li, ^{8}He +^{181}Ta reactions in the
  10–40 *A* MeV range of energies.
- The resulting experimental total cross sections of reaction ^{8}Li, ^{8}He + ^{28}Si are in good agreement with the literature results and cover the range of energies not investigated earlier. The larger total cross sections of reactions on ^{59}Co, and ^{181}Ta targets can be explained in a simple approximation by the larger sizes of these nuclei.
- The multiplicities of emitted neutrons are explained using fusion evaporation channels calculations.
- The neutron transfer and neutron remove channels are studied using numerical solving of time-dependent Schrödinger equation.

Thank You